Journal of Power Sources 242 (2013) 314–324

Contents lists available at SciVerse ScienceDirect

Journal of Power Sources

journal homepage: www.elsevier.com/locate/jpowsour

Thermal hydraulic behavior and efficiency analysis of an all-vanadium redox flow battery

Binyu Xiong [a], Jiyun Zhao [a,*], K.J. Tseng [a], Maria Skyllas-Kazacos [b], Tuti Mariana Lim [c], Yu Zhang [a]

[a] EXQUISITUS, Centre for E-City, School of Electrical & Electronic Engineering, Nanyang Technological University, Singapore 639798, Singapore
[b] School of Chemical Engineering, The University of New South Wales, UNSW Sydney, NSW 2052, Australia
[c] School of Civil and Environmental Engineering, Nanyang Technological University, Singapore 639798, Singapore

HIGHLIGHTS

- A thermal hydraulic model is developed for vanadium flow battery.
- The pump power is sensitive to hydraulic design and flow rates.
- Thermal hydraulic model is benchmarked with experimental data.
- Sensitivity of efficiencies on the temperature, current, and flow rate is studied.
- Optimal flow rates to reach highest battery efficiency are obtained.

ARTICLE INFO

Article history:
Received 2 April 2013
Received in revised form
19 May 2013
Accepted 21 May 2013
Available online 31 May 2013

Keywords:
Vanadium redox flow battery
Pump power losses
Thermal hydraulic modeling
Optimal flow rate
Battery efficiency

ABSTRACT

Vanadium redox flow batteries (VRBs) are very competitive for large-capacity energy storage in power grids and in smart buildings due to low maintenance costs, high design flexibility, and long cycle life. Thermal hydraulic modeling of VRB energy storage systems is an important issue and temperature has remarkable impacts on the battery efficiency, the lifetime of material and the stability of the electrolytes. In this paper, a lumped model including auxiliary pump effect is developed to investigate the VRB temperature responses under different operating and surrounding environmental conditions. The impact of electrolyte flow rate and temperature on the battery electrical characteristics and efficiencies are also investigated. A one kilowatt VRB system is selected to conduct numerical simulations. The thermal hydraulic model is benchmarked with experimental data and good agreement is found. Simulation results show that pump power is sensitive to hydraulic design and flow rates. The temperature in the stack and tanks rises up about 10 °C under normal operating conditions for the stack design and electrolyte volume selected. An optimal flow rate of around 90 $cm^3\ s^{-1}$ is obtained for the proposed battery configuration to maximize battery efficiency. The models developed in this paper can also be used for the development of a battery control strategy to achieve satisfactory thermal hydraulic performance and maximize energy efficiency.

1. Introduction

Large-capacity batteries for energy storage provide a feasible solution to implement renewable energies such as wind and solar, to counter their intermittent and unsteady characteristics. They can also serve as the key components in a smart grid that manages power flow. All-vanadium redox flow batteries (VRBs) initiated by Skyllas-Kazacos and co-workers [1–3] at University of New South Wales are successfully commercialized and highly competitive among various designs of redox flow batteries, with features such as flexibility for power and capacity design, elimination of electrolyte cross-contamination, high energy efficiency, low capital cost for large energy storage capacities, long cycle life of the electrolytes, etc. One critical aspect in battery design is the thermal modeling. Temperature needs to be controlled within the expected range since it affects the stability of electrolytes, the thermal dynamic properties of electrolytes, the resistivity of materials and therefore the overall efficiency of the VRB battery system.

* Corresponding author. Tel.: +65 6790 4508; fax: +65 6793 3318.
E-mail address: jyzhao@ntu.edu.sg (J. Zhao).

0378-7753/$ – see front matter © 2013 Elsevier B.V. All rights reserved.
http://dx.doi.org/10.1016/j.jpowsour.2013.05.092

Nomenclature

c	vanadium concentration (mol L^{-1})
f	friction factor
q	heat release
z	number of electron transferred in reaction
A	surface area (m^2)
C_p	specific heat of electrolyte (kJ kg K^{-1})
D_h	hydraulic diameter (m)
F	Faraday constant (C mol^{-1})
H	enthalpy (J)
I	current (A)
K	coefficient of form loss
L	length of pipes (m)
N	number of cells
P	power (W)
Q	flow rate (cm^3 s^{-1})
R	resistance (Ω)
Re	Reynolds number
S	entropy (JK^{-1})
SOC	state of charge
T	temperature (°C)
H	heat convection coefficient ($Wm^{-2}K^{-1}$)
V	volume of stack or tank (L)

Greek symbol

ε	carbon electrode porosity
μ	dynamic viscosity (cP)
ρ	electrolyte density (kg m^{-3})
θ	polypropylene thickness (m)

Subscript

ch	chemical reaction
min	minimal flow rate
t	tank
cell	cells in stack
c	charging
d	discharging
m	mean velocity in the channels
r	resistance
s	stack
+	positive side
−	negative side

The thermal stability of the electrolytes has been investigated at different temperatures and vanadium solution compositions since the 1980s. Skyllas-Kazacos [4] found the negative half-cell vanadium couples, V (II)/V (III) started to precipitate at temperature below 10 °C and the positive half-cell vanadium ion V (V) started to precipitate at above 40 °C when the vanadium concentration is 2 M or higher. Hence, extreme temperatures that affect the solubility limits of vanadium species should be avoided. Later, Kazacos et al. [5] optimized the electrolyte solutions containing 2 M V(V) in 4–5 M H_2SO_4 solution for increased stability and electrolyte conductivity. In order to achieve a greater temperature range, a lower vanadium ion concentration of 1.5–1.6 M can be used although this reduces the specific energy of the VRB. In Ref. [6], it was found that the increase of temperature led to better voltage efficiencies due to the rise in electrolyte conductivity and increased reaction kinetics. Besides, thermo-physical properties of electrolytes such as viscosity, density and specific heat are also temperature dependent.

Despite the above, only a few thermal models of VRBs have been developed. A model based on the conservation of mass, energy, charge and momentum was set up by Al-Fetlawi et al. [7]. Temperature distributions in the entire cell were obtained under different applied currents and flow rates, and the charge/discharge currents and flow rates were found to have significant effects on temperature rise and distribution. In Tang et al. [8,9], a dynamic thermal model was proposed based on conservation of energy to forecast the electrolyte temperature in the stack and tanks. Dynamic temperature changes of stack and tanks under different scenarios are simulated. These models neglected the impacts of pump energy losses on thermal modeling and battery efficiencies.

In this paper, pump power losses are included in the thermal model. An empirical method for loss measurement is firstly introduced according to the battery hydraulic design. After thermal model development, optimal operational flow rates are found for normal battery operation. To analyze battery efficiencies, factors such as temperature, optimal operational flow rates and charge–discharge currents are investigated.

2. Method of analyzing pressure drop and pump power

The pump power sustains constant flow rates of electrolytes through the cell stack and any energy losses are converted to heat that is carried out of the stack by the flow. In this paper, the pump power is referred to the actual work done by overcoming the flow resistances through the hydraulic loops, neglecting the heat dissipated in the atmosphere due to low electrical motor efficiency. The pump power is related to the pressure drop and flow rate Q and is given by [10],

$$P_{\text{pump}} = \Delta p \times Q \tag{1}$$

where $\Delta p = \Delta p_{\text{friction}} + \Delta p_{\text{form}}$.

The pump power is associated with two forms of energy loss in the hydraulic pipes and the stack. For steady-state flow of incompressible and viscous fluids in pipes, the friction pressure drop, $\Delta p_{\text{friction}}$, is attributed to the effect of viscosity due to the wall and shear stress within the fluid. In addition, a form loss, Δp_{form}, exists due to abrupt changes in flow direction or geometry. The pressure loss, including the friction pressure drop and the form loss, is analyzed under normal operation condition. The pump power can be obtained either experimentally or using empirical equations. In this study, the latter method is adopted.

2.1. The pressure drop in hydraulic circuits

The common components of the electrolyte hydraulic circuits in VRB system are bends, elbows and valves. These components lead to form loss in the pipes which occur whenever the flow changes its direction and velocity. Also the roughness of pipe wall and the fluid viscosity lead to friction loss. The pressure drop in the hydraulic circuits occurs when the electrolytes run through the pipes and elbows and enters the reservoirs. The pressure drop is related to the geometry of the hydraulic circuits, tanks and flow rates from Eqs. (2) and (3) given as follows,

The pressure drop across a channel is [11,12],

$$\Delta p_{\text{friction}} = f\frac{L}{D_h}\frac{\rho V_m^2}{2} \tag{2}$$

The form pressure drop is given by,

$$\Delta p_{\text{form}} = K\left(\frac{\rho V_m^2}{2}\right) \tag{3}$$

where V_m denotes the average flow velocity in the pipes.

2.2. The pressure drop in stack

The stack consists of several parallel aligned cells which are fabricated by a set of basic elements: ion exchange membranes, bipolar electrodes, end plates, carbon felt, and current collectors. The electrolytes in the stack flow through the inlet pipes which are distributed evenly into the flow channel in each cell. The electrolyte in a flow channel is simplified by flow through a rectangular channel regardless of the porosity of the electrodes. The electrolyte in a flow channel flow through a rectangular cell into the porous electrodes within the cell cavity and the pressure drop is estimated by adopting Kozeny-Carman law in Eq. (4) in Ref. [13].

$$\Delta P = \mu\left[\frac{K(1-\varepsilon)^2}{\varepsilon^3 d_f^2}\right]U_0 L \tag{4}$$

where ε denotes the porosity of carbon felt electrodes, d_f is a mean fiber diameter, K is the Kozeny-Carman coefficient for a fibrous medium and U_0 represents the superficial velocity in the cell. μ is the dynamic viscosity of electrolytes.

A typical diagram of a VRB stack structure is shown in Fig. 1. The overall stack friction pressure drop is estimated by evaluating three basic components: inlet pressure drop, outlet pressure drop and pressure drop in the channels, and then coupling them together.

The flow resistance R_s is introduced to evaluate the overall stack friction pressure drop and defined as,

$$R_s = \frac{\Delta P}{Q} \tag{5}$$

The flow resistance is considered as a property of each component with specific geometry, which is assumed to be constant. With relatively low velocity in the stack under normal operating condition, the flow is laminar. The friction loss exists in branches, channels and inlet/outlet manifolds, and can be estimated by Eq. (5) at various flow rates. Hydraulic resistance in the cells is analyzed by applying Eqs. (2)–(4) and the overall stack resistance is obtained by coupling parallel or series components together. The proposed method is validated in Ref. [14]. The form loss in the stack owing to sudden changes in flow direction in tees and channel geometry is included as well.

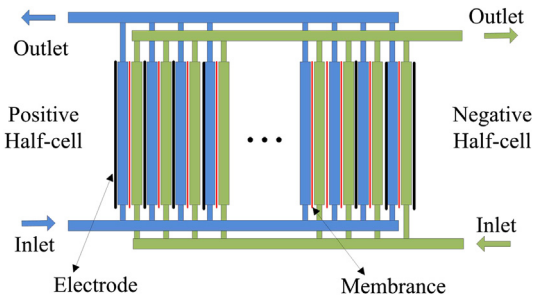

Fig. 1. Schematic of a stack structure in VRB.

3. Model assumptions and development

The dynamic thermal hydraulic modeling for the tanks and stack is based on the conservation of energy. The assumptions are:

1. Incompressible flow of the dilute solution.
2. Temperatures in stack and tanks are uniformly distributed.
3. The tank size and flow rates are identical in both positive and negative sides.
4. Steady-state flow without abrupt change of the current or flow rate.
5. Thermodynamic properties of electrolytes are constant at various temperatures.

The stack temperature is determined by four factors, the heat of electrolytes transferred from pipes, the natural convection heat dissipated to the surroundings, the power generated by internal resistance and chemical reaction heat released to the electrolytes. The energy equation in terms of the stack temperature T_s is shown in Eq. (6),

$$C_p\rho V_s\frac{dT_s}{dt} = Q_+C_p\rho(T_{p+}-T_s) + Q_-C_p\rho(T_{p-}-T_s) + H_sA_s(T_{air}-T_s) + P_R + P_{ch} \tag{6}$$

where P_R are the ohmic and overpotential losses in the stack which depend on the value of resistance and the applied currents during charge/discharge processes. P_{ch} denotes the chemical reaction heat generation/absorption during charge/discharge process. The ohmic power loss has the relationship shown as $P_R = I^2R$. H_sA_s is the term representing heat transfer in terms of nature convection at the stack.

The model development for pipe temperature of each side is similar to that of stack temperature, which is shown in Eqs. (7) and (8). The pump power is incorporated into the equations as well as the term of heat convection of pipes.

$$C_p\rho V_p\frac{dT_{p+}}{dt} = Q_+C_p\rho(T_{t+}-T_{p+}) + Q_+C_p\rho(T_s-T_{p+}) + H_pA_p \times (T_{air}-T_{p+}) + P_{pump+} \tag{7}$$

$$C_p\rho V_p\frac{dT_{p-}}{dt} = Q_-C_p\rho(T_- - T_{p-}) + Q_-C_p\rho(T_s - T_{p-}) + H_pA_p \times (T_{air} - T_{p-}) + P_{pump-} \tag{8}$$

The tank temperature in Eqs. (9) and (10) is affected by the heat convection to the surroundings and pipe temperature.

$$C_p\rho V_{t+}\frac{dT_{t+}}{dt} = Q_+C_p\rho(T_{p+} - T_{t+}) + H_tA_t(T_{air} - T_{t+}) \tag{9}$$

$$C_p\rho V_{t-}\frac{dT_{t-}}{dt} = Q_-C_p\rho(T_{p-} - T_{t-}) + H_tA_t(T_{air} - T_{t-}) \tag{10}$$

The state-space model of the positive side of the VRB system is represented by,

$$\dot{x} = Ax + Bu$$

$$y = Cx + Du$$

where the state vector, $x = \begin{bmatrix} T_s \\ T_{p+} \\ T_{t+} \end{bmatrix}$, the input signal vector, $u = \begin{bmatrix} I^2R \\ T_{air} \\ P_{pump} \\ P_{ch} \end{bmatrix}$,

$$A = \begin{bmatrix} -\frac{Q_+ + Q_-}{V_s} - \frac{H_sA_s}{C_p\rho V_s} & \frac{Q_+ + Q_-}{V_s} & 0 \\ \frac{Q_+}{V_p} & -\frac{Q_+ + Q_-}{V_p} - \frac{H_pA_p}{C_p\rho V_p} & \frac{Q_+}{V_p} \\ 0 & \frac{Q_+}{V_{t+}} & -\frac{Q_+}{V_{t+}} - \frac{H_tA_t}{C_p\rho V_{t+}} \end{bmatrix},$$

$$B = \begin{bmatrix} \frac{1}{C_p\rho V_s} & \frac{H_sA_s}{C_p\rho V_s} & 0 & \frac{1}{C_p\rho V_s} \\ 0 & \frac{H_tA_t}{C_p\rho V_p} & \frac{1}{C_p\rho V_p} & 0 \\ 0 & \frac{H_tA_t}{C_p\rho V_{t+}} & 0 & 0 \end{bmatrix}$$

$$C = \begin{bmatrix} 1 & 0 & 0 \\ 0 & 1 & 0 \\ 0 & 0 & 1 \end{bmatrix}, \quad D = 0$$

The temperature of the stack, pipes, tanks can be estimated by applying Eqs. (6)–(10). The terms such as chemical reaction heat generation/absorption, pump power, and resistance power loss and heat convection rates of stack, pipes and tank to atmosphere are analyzed in details below.

3.1. Pump power investigation

The consumption of pump power relates to flow rate and the design of stack and hydraulic circuits as shown in Eqs. (2) and (3). In Eq. (2), the hydraulic diameter, D_h, is defined as,

$$D_h = 4\frac{A_w}{P} \tag{11}$$

where A_w is the cross sectional area and P is the wetted perimeter of the cross-section.

For laminar flow in circular pipes, the friction factor can be determined from

$$f = \frac{64}{Re} \tag{12}$$

where

$$Re = \frac{\rho D_h V_m}{\mu} \tag{13}$$

For laminar flow, the value of $f \cdot Re$ for fully developed flow in rectangular channel is given in Kays and Crawford [15]. For turbulent flow in circular pipes, the friction factor can be determined from the Moody chart [16]. The flow rates in the pipes are with low velocity at normal operating point and the fluid is assumed to be laminar flow.

3.2. Convection heat transfer for the stack and tanks

Heat exchanges occur spontaneously on the surface of the stack, H_sA_s, and tanks, H_tA_t, in terms of the natural convection of air and electrolyte. The overall heat transfer of the tanks and stack are determined based on the areas of top or bottom wall and side wall and the heat transfer coefficient of stack with calculation are given by [8],

$$H_sA_s = 2 \times H_{1,s}A_{1,s} + 4 \times H_{2,s}A_{2,s}$$

$$H_pA_p = \pi \times (D/2)^2 \times L_p \times H_p$$

and

$$H_tA_t = 2 \times H_{1,t}A_{1,t} + 4 \times H_{2,t}A_{2,t} \tag{14}$$

where $H_{1,t}$, $H_{2,t}$, $H_{1,s}$, $H_{2,s}$ denote the heat transfer coefficients of the top or bottom wall and side wall of tanks and stack respectively. H_p denotes the heat transfer coefficients of the pipes. $A_{1,t}$, $A_{2,t}$, $A_{1,s}$, $A_{2,s}$ are the corresponding areas. D denotes the pipe diameter.

The value of heat transfer coefficient is shown in Table 1 with respect to the configuration of VRB battery shown in Fig. 3. The heat convection coefficients of rectangular walls of the tanks and stack are determined by series of heat transfer coefficients of air, polypropylene and electrolyte inside the tank. The heat convective capacity is calculated by the sum of thermal resistance of three layers. The general equations are shown below,

$$H = \frac{1}{1/h_1 + \theta/\kappa + 1/h_2} \tag{15}$$

where h_1, h_2 are convection heat transfer coefficients for inner and outer surfaces, θ denotes the polypropylene thickness, κ denotes the polypropylene conductivity.

The heat transfer coefficient h_1, h_2 of each surface of the tank and stack is calculated by

$$h = Nu\frac{k}{x} \tag{16}$$

where k denotes the thermal conductivity of the electrolyte, Nu denotes the Nusselt number, and x denotes the characteristic length. For natural convection, the Nusselt number is determined by the empirical equation in Eq. (17),

Table 1
Specifications in VRB simulation.

Symbol	Value
ρ	1400 kg m^{-3}
c	1.5 M
θ	0.01 m
κ	0.16 Wm^{-1} K^{-1}
ε	0.68
μ	7 cP
d_f	30×10^{-6} m
C_p	3200 kJ kg^{-1} K^{-1}
H_sA_s	1.78 J K^{-1} s^{-1}
H_tA_t	0.7 J K^{-1} s^{-1}
H_pA_p	2.07 J K^{-1} s^{-1}
N	14
V_t	7.4 L
V_s	0.6 L
R_c	0.015 Ω
R_d	0.024 Ω

$$\mathrm{Nu} = m\mathrm{Ra}^n \tag{17}$$

where the Rayleigh number Ra is related to the Grashof number Gr and the Prandtl number Pr of the fluid, which can be expressed as,

$$\mathrm{Ra} = \mathrm{Gr}\,\mathrm{Pr} = \frac{g\beta\Delta T x^3}{\upsilon^2}\,\frac{C_p\mu}{k} \tag{18}$$

where g denotes the gravity acceleration, υ denotes the kinematic viscosity, β denotes the volumetric thermal expansion coefficient. The values of the constants m and n in Eq. (17) are specific to the category of convection.

3.3. Chemical reaction heat

The reactions on positive and negative electrodes are shown respectively as follows [17],

$$\mathrm{VO}^{2+} + \mathrm{H_2O} \underset{\text{discharge}}{\overset{\text{charge}}{\rightleftarrows}} \mathrm{VO_2^+} + 2\mathrm{H^+} + \mathrm{e^-} \tag{19}$$

$$\mathrm{V}^{3+} + \mathrm{e^-} \underset{\text{discharge}}{\overset{\text{charge}}{\rightleftarrows}} \mathrm{V}^{2+} \tag{20}$$

The heat generation by chemical reactions can be calculated by the entropy change according to Table 3 [14].

The minimal amount of heat released during discharge is obtained by,

$$\begin{aligned} q &= T\Delta S = T\Big(\sum S_{\text{products}} - \sum S_{\text{reactants}}\Big) \\ &= T\Big(S^{2+}_{\mathrm{VO}} + S^{3+}_{\mathrm{V}} + S_{\mathrm{H_2O}} - S^{2+}_{\mathrm{V}} - S^{+}_{\mathrm{VO_2}} - 2S^{+}_{\mathrm{H}}\Big) \end{aligned}$$

The heat released when a discharging current I is applied is obtained by $P_{\mathrm{ch}} = qn = T\Delta Sn$ and $I = znF$, where n denotes the consumption rate of vanadium species, z denotes number of electron transferred in reaction, and F is the Faraday constant with a value of 96,500 C mol^{-1}.

3.4. Electrolyte flow rate

Electrolyte flow rate is a unique variable for flow batteries. The concentration of active species in the stack is related to the flow rates, which is shown in Eq. (21),

$$c_{\mathrm{s,out}} = c_{\mathrm{s,in}} \pm \frac{I}{zFQ_{\mathrm{cell}}} = \mathrm{SOC} \times c_{\mathrm{in}(0)} \pm \frac{I}{zFQ_{\mathrm{cell}}} \tag{21}$$

where $c_{\mathrm{s,out}}$ and $c_{\mathrm{s,in}}$ denotes the output and input vanadium concentrations of a cell respectively. The state of charge (SOC) is limited within the range of 10%–90%. N denotes the number of cells numbers.

In the minimal flow rate condition, the active vanadium species will be totally depleted when exiting the cell. For good mass transport rates however, the electrolyte flow rate must exceed the minimal flow rates for the particular current and SOC of the cell where it is defined at $c_{\mathrm{s,out}} = 0$, whence

$$Q_{\mathrm{s,min}} = N\frac{I}{zF\mathrm{SOC}c_{\mathrm{in}}} \tag{22}$$

In practical applications, high battery efficiency is desirable to reduce operating costs and it is necessary to find out optimal flow rates at which the highest efficiency is attained. At the optimal flow rates, VRBs can deliver the maximum stack energy during the discharge process while absorbing the minimal battery energy during the charging process. The schematic of power flow of VRBs is shown in Fig. 2. The criteria for optimal flow rates are to maximize the battery power during discharge while minimize the battery power during charge. The relationship between battery energy, stack energy and pump energy is shown in Eq. (23).

$$E_{\mathrm{battery}} = \begin{cases} \max(E_{\mathrm{stack}} - E_{\mathrm{pump}}) = \max\left(\int P_{\mathrm{stack}}\mathrm{d}t - \int P_{\mathrm{pump}}\mathrm{d}t\right) & \text{during discharge} \\ \min(E_{\mathrm{stack}} + E_{\mathrm{pump}}) = \min\left(\int P_{\mathrm{stack}}\mathrm{d}t + \int P_{\mathrm{pump}}\mathrm{d}t\right) & \text{during charge} \end{cases} \tag{23}$$

4. Battery performance and efficiencies

Temperature and electrolyte flow rate affect battery performance and its efficiency. An increase in flow rate leads to an increase in battery capacity, but a decrease in system efficiency [18]. It is crucial to analyze energy efficiency and battery efficiency under various flow rates and temperatures. The definitions of energy efficiency and battery efficiency are described in Eqs. (24) and (25) respectively.

$$\eta_{\mathrm{e}} = \frac{\text{Discharged Energy}}{\text{Charged Energy}} = \frac{\int P_{\mathrm{stack,d}}\mathrm{d}t}{\int P_{\mathrm{stack,c}}\mathrm{d}t} \tag{24}$$

$$\begin{aligned} \eta_{\mathrm{battery}} &= \frac{\text{Discharged Energy} - \text{Pump Energy}}{\text{Charged Energy} + \text{Pump Energy}} \\ &= \frac{\int\left(P_{\mathrm{stack,d}} - P_{\mathrm{pump,d}}\right)\mathrm{d}t}{\int\left(P_{\mathrm{stack,c}} + P_{\mathrm{pump,c}}\right)\mathrm{d}t} \end{aligned} \tag{25}$$

The battery voltage is described according to Nernst Equation in Eq. (26),

$$U_{\mathrm{battery}} = E_0 + N\frac{2RT}{F}\ln\left(\frac{c_{\mathrm{vo}_2^+,\mathrm{c}}}{1 - c_{\mathrm{vo}_2^+,\mathrm{c}}}\right) \pm \mathrm{Ri} \tag{26}$$

where E_0 denotes the standard potential for a redox reaction when the activity of vanadium species is unity. E_0 is affected by temperature. The term in bracket denotes the concentrations of vanadium species in cells, which are dependent on the SOC, the current and the flow rates. R denotes the equivalent internal resistance represents ohmic losses. N denotes the cell number.

Temperature dependent parameters such as reaction overpotential η_{act} and standard potential E_0 in Nernst equation are included in the model. In the thermal model, the reaction overpotential is described as Bulter-volmer relation in Eq. (27),

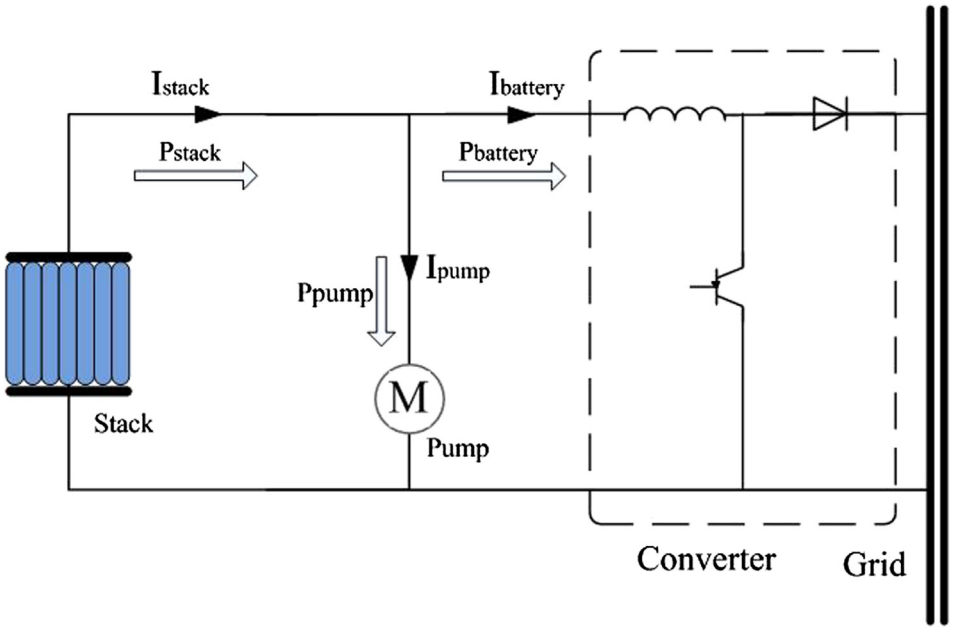

Fig. 2. Schematic of VRB during charge.

$$I = I_0\left(\exp\left(\frac{\alpha z F \eta_{act}}{RT}\right) - \exp\left(\frac{-(1-\alpha) z F \eta_{act}}{RT}\right)\right) \quad (27)$$

where I_0 is the exchange current, α denotes the charge transfer coefficient.

Standard potential E_0 is dependent with temperature and have a relationship in Eq. (28) in [14],

$$\frac{\partial E_0}{\partial t} = -\frac{1}{nF}\left(\frac{\partial \Delta G}{\partial T}\right) \quad (28)$$

where ΔG denotes the standard Gibbs free enthalpy. ΔS denotes the standard reaction entropy. These values are stated in Table 3.

5. Simulation results

A kilowatt class VRB stack is analyzed and simulated with charge–discharge characteristics for battery modeling. The simulation is conducted by adopting a 1 kW VRB system with 14 cells in the stack. The electrolyte solution contains 1.5 M vanadium species and 3 M total sulfate at both negative and positive sides. The electrolyte has a density around 1400 kg m^{-3}. The estimated dynamic viscosity of V (IV) in a 3 M H_2SO_4 solution is around 8 cP [19], and the dynamic viscosity of V (V) in total sulfates concentration of 3 M is 7 cP [20,21]. The assumed dynamic viscosity of positive and negative electrolytes is 8 cP. The specific heat of vanadium electrolyte is 3.2 J $g^{-1}K^{-1}$ [8]. The tank reservoir contains 7.4 L electrolytes. The active electrode area is 875 cm^2. The constructed battery has the specifications in Table 1 of Ref. [22].

5.1. Pump power losses and hydraulic design

Pump power is analyzed by adopting the method above. Fig. 3 plots the configuration of the VRB system. The electrolyte flows through each cell with the design of length $L = 0.2$ m, thickness $W = 0.004$ m, and height $H = 0.44$ m.

5.1.1. Case study

The evaluation of pump power at flow rate $Q = 125$ cm^3 s^{-1} is attached as a case shown below. Table 2 [23] lists the coefficients of form loss for the commonly used components.

For each cell, from Fig. 3,

$$A_{cell} = 0.0002\ m^2; \quad Re = \rho D_{cell} V_{cell}/\mu;$$
$$V_{cell} = Q/A_{cell}; \quad f_{cell} = 56/Re$$

$$\text{At } Q = 125\ cm^3 s^{-1}, \quad \varepsilon = 0.68, \quad d_f = 3\times 10^{-5}\ m,$$
$$Sv = 2\times 10^6, \quad K = 5;$$

$$\Delta p_{cell} = \mu K(1-\varepsilon)^2/\left(\varepsilon^3 d_f^2\right) \times U_0 \times L = 6.25\times 10^4\ Pa;$$

$$R_{ch} = \Delta p_{cell}/Q = 2.7863\times 10^{10}\ Pas\ m^{-3};$$

Similarly, $D_{pipe} = 0.01$ m,

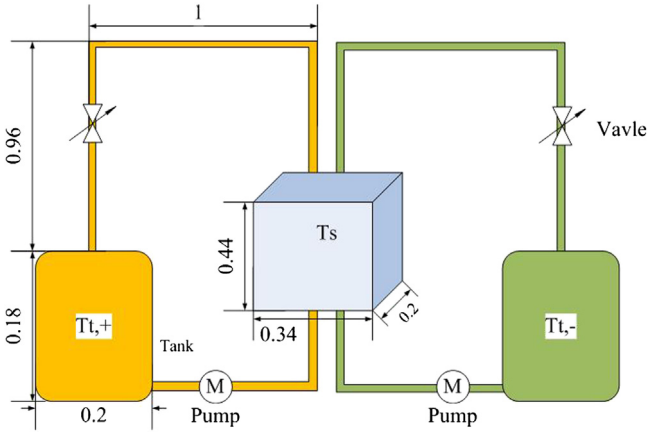

Fig. 3. Configuration of VRB system (metric).

Table 2
Form loss coefficients for diverse bends, elbows and valves.

Component	K (flanged)	K (threaded)
Regular 90° elbow	0.3	1.5
Long radius 90° elbow	0.2	0.7
Long radius 45° elbow	0.2	0.4
180° return bend	0.2	1.5
Line flow tee	0.2	0.9
Brand flow tee	1	2
Gate valve		0.15 (fully open)

$$R_{branch} = \Delta p_{branch}/Q = 3.17 \times 10^6 \text{ Pas m}^{-3}$$

With 14 cells in parallel, the overall hydraulic resistance according to Fig. 3, the overall stack friction resistance has a value of $R_{stack} = 5.004 \times 10^8$ Pas m^{-3}.

At $Q = 125$ cm^3 s^{-1}, $\Delta p_{friction,stack} = R_{stack}Q = 6.25 \times 10^4$ Pa;

Line flow tee coefficient $K_1 = 0.9$; Brand flow tee coefficient $K_2 = 2$, from Table 2;

$$\Delta p_{form,stack} = \sum\left(K_1 \rho V_{branch}^2/2 + K_2 \rho V_{branch}^2/2\right) = 8.16 \times 10^3 \text{ Pa}$$

The overall stack pressure drop is, $\Delta p_{stack} = \Delta p_{form,stack} + \Delta p_{friction,stack} = 7.06 \times 10^4$ Pa.

For hydraulic circuits, from Fig. 3,

$$\Delta p_{friction,hydra} = f_{pipe} L_{pipes}/D_{pipe} \times \rho V_{pipe}^2/2 = 1.28 \times 10^4 \text{ Pa}$$

The form loss, the elbow friction coefficient $K_{elbow} = 1.5$, from Table 2; and form loss coefficient when entering or exiting the reservoir $K_{tank} = 0.97$

$$\Delta p_{form,hydra} = 3 \times K_{elbow} \rho V_{pipe}^2 + 2 \times K_{elbow} \rho V_{pipe}^2 = 3.18 \times 10^4 \text{ Pa}$$

$$\Delta p_{hydra} = \Delta p_{form,hydra} + \Delta p_{friction,hydra} = 4.46 \times 10^4 \text{ Pa}$$

$$P_{pump} = \left(\Delta p_{stack} + \Delta p_{hydra}\right) Q \times 2 = 28.85 \text{ W}$$

From the case above, the stack pressure drop depends on the large hydraulic resistances of porous carbon electrodes. The hydraulic circuit pressure drop is attributed to the form loss depending on flow rates and pipe diameters. The pump power can be reduced with well designed hydraulic circuits from Fig. 4.

It is necessary to estimate the pump power under various flow rates and designs. Hydraulic designs with different pipe dimensions are discussed. The pump power losses are illustrated in Fig. 4. The pump power increases quadratically with the increase of flow rates. Pipe diameters also affect pump power losses significantly. Pumps tend to consume a large amount of energy for small

Table 3
Thermodynamical data for vanadium compounds at 298.15 K.

Formula	State	ΔH_f (kJ mol^{-1})	ΔG_f (kJ mol^{-1})	S_f (J mol^{-1}K^{-1})
V^{2+}	aq	(−226)	−218	(−130)
V^{3+}	aq	(−259)	−251.3	(−230)
VO^{2+}	aq	−486.6	−446.4	−133.9
VO_2^+	aq	−649.8	−587.0	−42.3
H_2O	aq	−285.8	−237.2	69.9
H^+	aq	0	0	0

Note: values in parentheses are estimated.

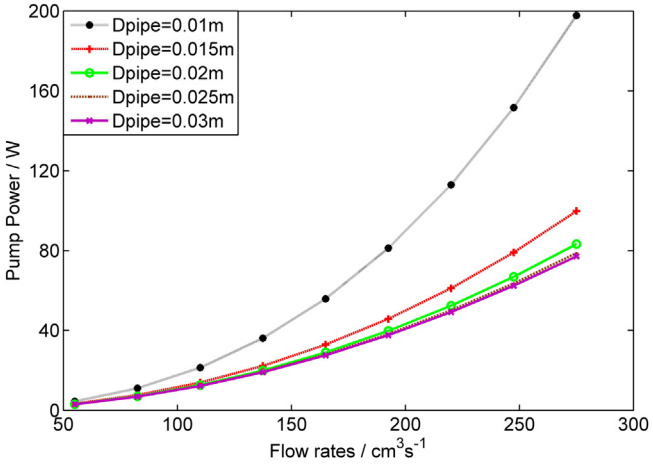

Fig. 4. Pump power with different hydraulic designs.

pipe diameters due to high friction loss. The pump power is remarkably reduced in a relatively big pipe dimension with slow electrolyte flow through the channels. This may happen during the startup of the battery, low SOC, or for sudden changes in charging/discharging currents. In practice, the operating flow rate is around 50–300 cm^3 s^{-1} for the current stack design and configuration. Fig. 4 shows that pump power will be less than 20 W even with a small pipe diameter. If the stack and hydraulic circuits are well designed, the pumps consume negligible power under normal conditions.

5.2. Model validation and sensitivity analysis

In practice, the surrounding temperature may vary during a day and a year, the electrolyte temperature in the stack under various surrounding temperatures is investigated as well. The thermal model is benchmarked with experiment conducted in Ref. [24] under surrounding temperature of −5 °C, 5 °C, 15 °C and 25 °C with current density ranging from 50–80 mA cm^{-2}. The results are shown in Fig. 5. The grey area in Fig. 5 shows the temperature region that the stack temperature eventually reaches. The result indicates that stack temperature rises about 10 °C under each constant surrounding temperature. Simulated data in green and red color follows well with the trends of the experimental data

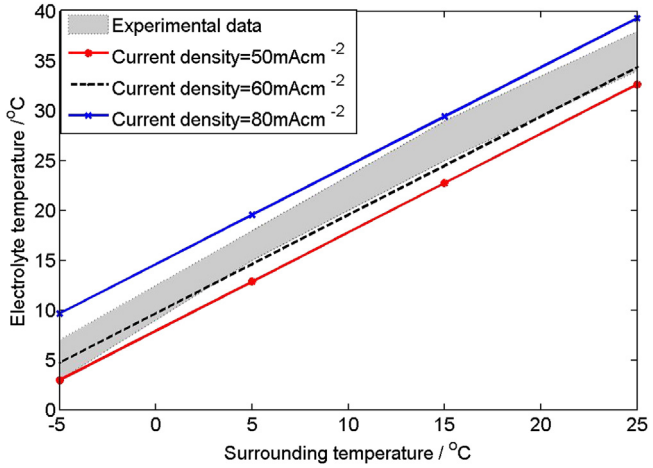

Fig. 5. Thermal model validation under various surrounding temperatures and current densities.

from Ref. [24], which validates the thermal modeling of stack. The electrolyte temperature rises up constantly around 10 °C respect to the surrounding temperature with a range of −5 °C to 25 °C, which indicates that the model is not sensitive to the ambient temperature. Also, it is found that the estimated temperature has relative big errors when current density reaches to the experimental limits.

5.3. Stack temperature investigation

The simulation is conducted to model the dynamic change of stack temperature under various flow rates. The initial temperature of the VRB system is set to 25 °C while the surrounding temperature remains constant at 25 °C. Fig. 6 shows the stack temperature at a flow rate of 125 $cm^3\ s^{-1}$ and current density of 50 mA cm^{-2}. The stack temperature reaches to 32 °C with a fluctuation of 1 °C , a temperature rise of 7 °C in the stack. The temperature rise attributes to resistive heat generation and pump power heat loss. The temperature fluctuation in one cycle is caused by the variation of resistance and the heat release and absorption in chemical reaction during charging and discharging process.

The stack temperature is investigated under various flow rates and charge–discharge currents and the result is illustrated in Fig. 7. The initial temperature of VRB and the surrounding air temperature is 25 °C. As the flow rates increases from 55 $cm^3\ s^{-1}$ to 200 $cm^3\ s^{-1}$, the stack temperature rises up about 5 °C in response to the increase of pump losses. Three charge–discharge currents, 30 mA cm^{-2}, 50 mA cm^{-2} and 70 mA cm^{-2} are employed in the simulation. The stack temperature increases as high as 40 °C at currents of 70 mA cm^{-2} and flow rates of 192.5 $cm^3\ s^{-1}$. For high charge–discharge currents and flow rates, the temperature rise is obvious and it is mainly caused by the heat release of ohmic resistance and pump power losses.

5.4. Stack, pipe and tank temperature

The temperature fluctuation for one cycle in the stack, pipe and tanks is plotted in Fig. 8. The temperatures of the stack, pipe and tanks are measured respectively at the charging and discharging current density of 60 mA cm^{-2}. The corresponding figure shows

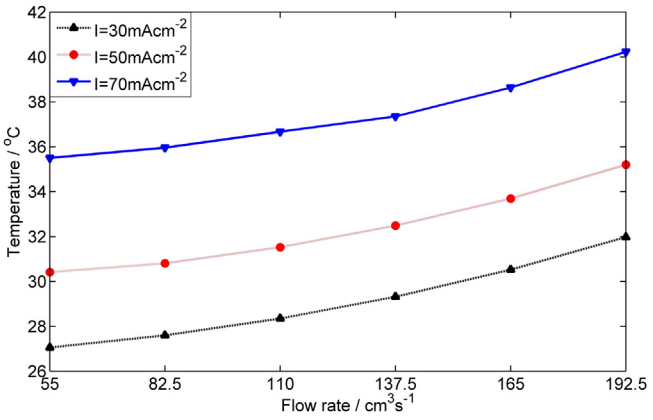

Fig. 7. Stack temperature under various flow rates and current densities.

that there is a slight temperature variation between the stack, pipe and tanks. The figure indicates the stack remains the highest temperature along the whole process. It is worth noting that the pipe temperature is lower than tank temperature during discharge in steady-state, which can be explained as the pipe possesses large heat convection rate and leads to the temperature drop quickly before entering the tanks. Besides, the curve of tank temperature is relatively smooth compared with that of pipes and stack. The phenomenon is reasonable due to the large size of tank and big specific heat value.

5.5. Battery electrical characteristics under different flow rates and temperatures

The effects of flow rates and temperatures on battery electrical characteristics are analyzed in the following section. The stack voltage is observed with the flow rates varying from 55 $cm^3\ s^{-1}$ to 275 $cm^3\ s^{-1}$ at current density of 60 A cm^2. The result is presented in Fig. 9. High electrolyte flow rates deliver much vanadium species into cells and reduce the concentration overpotential, which contributes to a high discharge stack voltage and a low charging stack

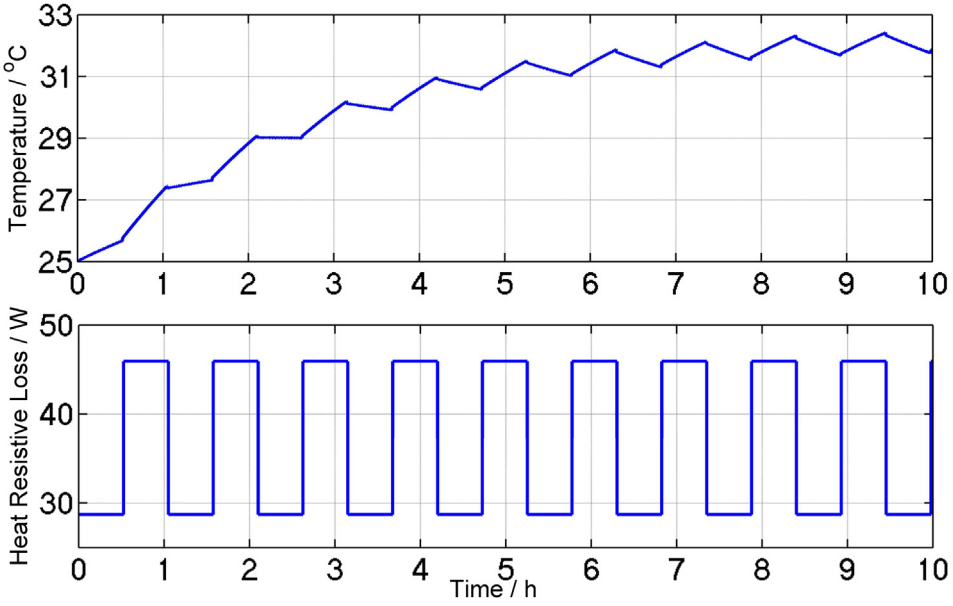

Fig. 6. Stack temperature at flow rate of 125 $cm^3\ s^{-1}$, current density of 50 mA cm^{-2}.

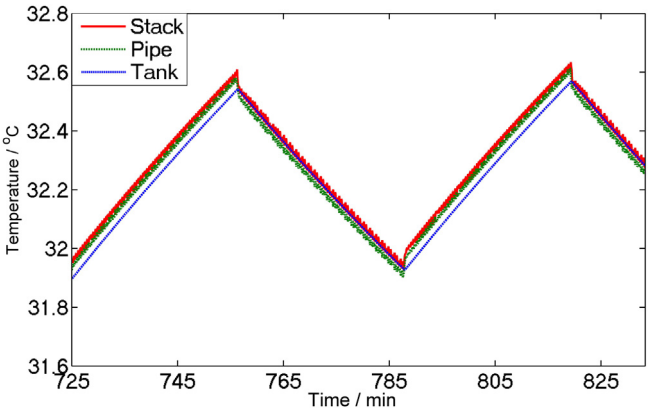

Fig. 8. Temperature in the stack, pipe and tanks in steady state.

voltage according to Eq. (26). The capacity of VRB is determined by the charge–discharge time at the same applied currents. It is evident that charge–discharge time is increased under high flow rates from the figure. Thus, high flow rates increase the capacity of VRB at the same charge–discharge current.

The stack voltage is simulated under temperatures from −5 °C to 35 °C. Previous studies in Ref. [25] shows that the standard potential is temperature dependent and has a negative linear relationship between them. Fig. 10 demonstrates the stack voltage under various stack temperatures. It is expected that the stack voltage will drop as the temperature increases since the activation overpotential for the electrode reactions decreases in response to improved reaction kinetics. Additionally, temperature alters permeability of the membrane. High temperature speeds up the diffusion rates of vanadium ions through membrane and therefore leads to a reduction of the concentrations of active vanadium ions that also releases energy from the resultant self-discharge reactions [9]. Although this effect has been ignored in the present model, it has been shown to be quite significant.

5.6. Optimal flow rates

As mentioned above, a fast flow rate increases the stack voltage as well as the battery capacity at the expense of greater energy consumption by the pumps. Using flow rates acquired from Eq. (23), the optimal flow rates are calculated during discharge at each

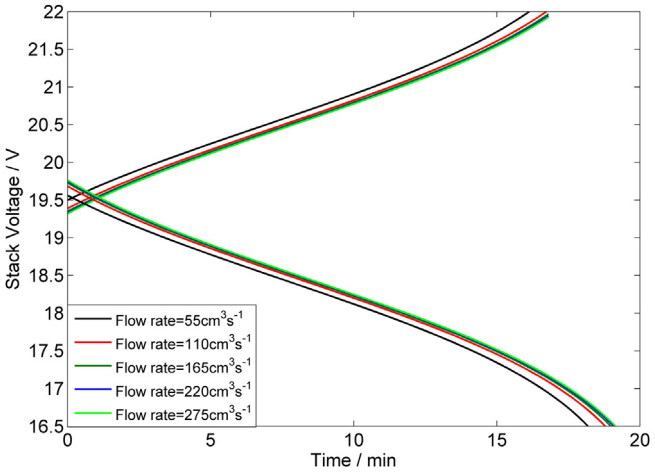

Fig. 9. Stack voltage under various flow rates at current density of 50 A cm^{-2}.

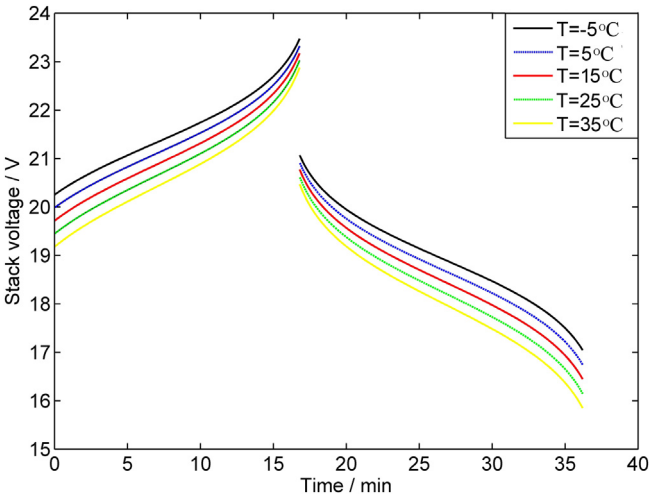

Fig. 10. Stack voltages under various surrounding temperature.

SOCs when $I = 60$ A and the results are presented in Fig. 11. The optimal flow rates corresponding to the maximum power points are marked in the red triangle. It can be observed that the optimal flow rates are around 90 cm^3 s^{-1} for the present battery configuration. Note that battery requires a faster optimal flow rate at lower or higher SOCs to replenish the scarce vanadium species in the solution. Fig. 12 shows the optimal flow rates at currents from 40 A to 80 A during charge. The curves describe the optimal flow rates at each charge current. From the figure, large currents consume the vanadium ions quickly and thus require a fast flow rate. These data can be facilitated for battery flow rate control as previously described by Skyllas-Kazacos et al. [26].

5.7. Energy efficiency and battery efficiency

According to Eqs. (24) and (25), the energy efficiency and battery efficiency are analyzed under various flow rates and surrounding temperatures in this section. Tables 4 and 5 list the efficiencies respectively. The energy efficiency in Fig. 13 improves gradually with the increase in flow rates. The battery efficiency reaches 84.10% at around 90 cm^3 s^{-1} at 70 mA cm^{-2} and declines at high flow rates due to the increasing pump energy consumption.

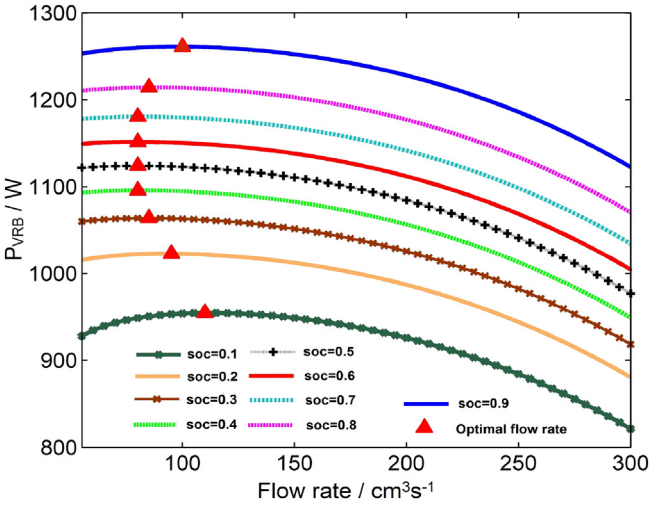

Fig. 11. Optimal flow rates during discharge when $I = 60$ A.

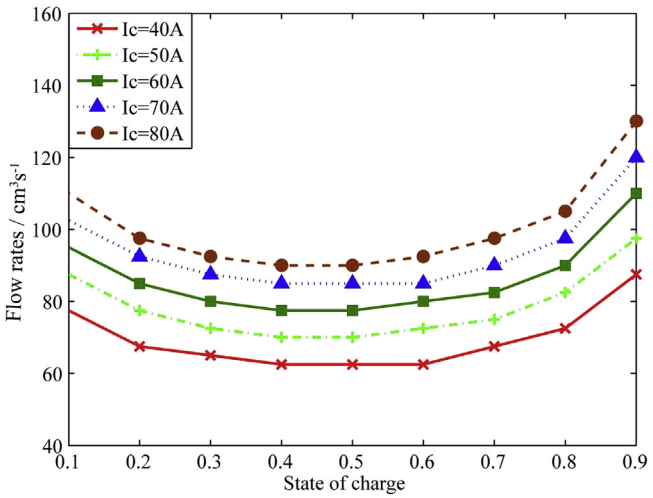

Fig. 12. Optimal flow rates under various currents during charge.

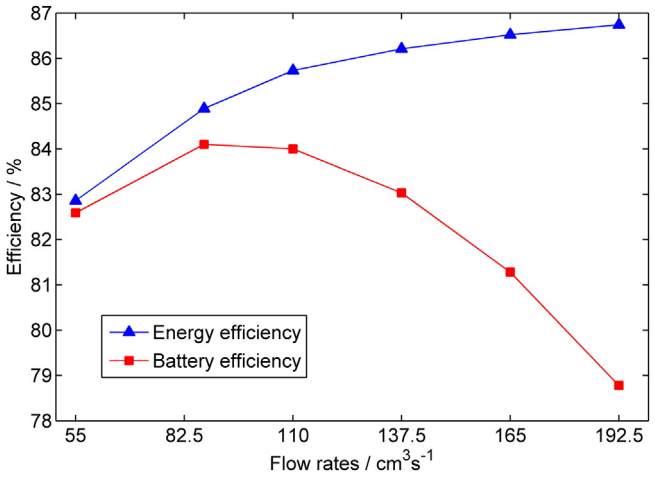

Fig. 13. Energy and battery efficiencies under various flow rates.

For practical operation, flow rates can be tuned to the optimal flow rates to achieve high battery efficiency. The effect of temperature on efficiency is analyzed and the results are shown in Table 5. It can be seen that energy efficiency and battery efficiency increase as the temperature increases in the range of −5 °C to 35 °C.

6. Discussion

The electrolyte temperature is affected by the current, surrounding temperature, flow rates and pump power losses. The pump power losses are deemed as a negligible term in the previous modeling, however, it is found that about 45 W of pump power consumption at the flow rate of around 200 $cm^3\ s^{-1}$, which is an indispensable part of power converted to heat for temperature rise of electrolyte. The pump power losses rely on hydraulic design of the battery and increase dramatically in response to the increased flow rate. So it is critical to select the appropriate parameters such as pipe diameter, stack cell dimension and tank size. Simulation results show that a large pipe diameter will decrease the pump power loss drastically as expected. The pressure drop in the common manifold that feeds each cell in the stack has been neglected and any increases in this will lead to increased shunt current and internal self-discharge reaction losses that will in turn lead to increased heat generation. To simplify pump power calculation, the cell cavity flow channels in the stack are treated as the rectangular channels considering the porosity of the felt electrodes. Fast flow rates enhance electrical characteristics for charge–discharge cycle while degrade overall battery efficiency due to pumping energy losses. The parameters for electrical model such as charge/discharge resistance in Nernst equation are estimated by least square method and verified by experimental data in Ref. [22]. One strategy proposed in this paper for battery control is to control the flow rate at optimal flow rates to achieve top battery efficiency. The method to obtain optimal flow rates is straightforward. In addition, for an accurate thermal model, further investigations are needed to take into account the factors such as self-discharge including shunt current and membrane diffusion processes and side reactions which deteriorate battery capacity and reduce the coulomb efficiency. The effects of temperature on battery efficiency need to be validated with experimental data in the future.

Table 4
Battery performance under various flow rates (at current of 70 mA cm^{-2} and temperature of 25 °C).

Flow rate($cm^3\ s^{-1}$)	55	87.5	110	137.5	165	192.5
Energy efficiency (%)	82.86	84.89	85.73	86.21	86.52	86.74
Battery efficiency (%)	82.59	84.10	84.00	83.03	81.28	78.78

Table 5
Battery performance under various temperatures (at current of 70 mA cm^{-2} and temperature of 25 °C).

Temperature (°C)	−5	5	15	25	35
Energy efficiency (%)	85.19	85.52	85.85	86.19	86.54
Battery efficiency (%)	82.89	83.19	83.49	83.80	84.12

7. Conclusion

The effect of pump power losses on the electrolyte temperature is not negligible at high flow rate. The present model includes the pump power energy consumption in the thermal modeling and an empirical method is proposed on the basis of battery configuration. As expected, temperature rise relates to flow rates and charge/discharge current. The simulation results show that stack temperature will increase at an average of 10 °C in respect to the selected model and has been verified by experimental data. The proposed model is accurate and can be utilized to forecast the stack and tank temperature dynamically. It is also found that the pump power is very sensitive to the flow rate and hydraulic design. The pump power remains low under low electrolyte flow rates, but will increase quadratically as the flow rate increases. Besides, there is a slightly difference between temperatures of the stack, pipe and tank from simulation results due to the good heat transfer ability of fast flow rates. Battery efficiency and energy efficiency are analyzed under different temperatures and flow rates. Energy efficiency is improved about 4% with the flow rates ranging from 55 $cm^3\ s^{-1}$ to 192.5 $cm^3\ s^{-1}$ while battery efficiency firstly increases at the optimal flow rate and then drops down about 5% due to large pump power losses. Energy efficiency and battery efficiency are improved about 1.23% at temperature range of −5 °C to 35 °C.

To achieve highest battery efficiency, the optimal flow rates are proposed by maximizing the discharge energy and minimizing charging energy during one cycle. The optimal flow rates vary around 90 $cm^3\ s^{-1}$ in respect to SOCs in the proposed battery configuration. Thus, it is reasonable to control the battery at these optimal flow rates. Hence, this paper presents the method of pump power calculation and flow rate optimization with the objective of obtaining insights in better hydraulic circuit design, and a correlation between the operating flow rate and temperature changes in the stack, pipe and tanks.

Acknowledgement

This research is funded by the Republic of Singapore's National Research Foundation through a grant to the Berkeley Education Alliance for Research in Singapore (BEARS) for the Singapore-Berkeley Building Efficiency and Sustainability in the Tropics (SinBerBEST) Program. BEARS has been established by the University of California, Berkeley as a center for intellectual excellence in research and education in Singapore.

References

[1] M. Skyllas-Kazacos, C. Menictas, M. Kazacos, J. Electrochem. Soc. 143 (1996) L86–L88.
[2] M. Skyllas-Kazacos, G. Kazacos, G. Poon, H. Verseema, Int. J. Energy Res. 34 (2010) 182–189.
[3] M. Skyllas-Kazacos, M.H. Chakrabarti, S.A. Hajimolana, F.S. Mjalli, M. Saleem, J. Electrochem. Soc. 158 (2011) R55–R79.
[4] M. Kazacos, M. Cheng, M. Skyllaskazacos, J. Appl. Electrochem. 20 (1990) 463–467.
[5] M. Skyllas-Kazacos, M. Kazacos, J. Power Sources 196 (2011) 8822–8827.
[6] G. Kear, A.A. Shah, F.C. Walsh, Int. J. Energy Res. 36 (2012) 1105–1120.
[7] H. Al-Fetlawi, A.A. Shah, F.C. Walsh, Electrochim. Acta 55 (2009) 78–89.
[8] A. Tang, S.M. Ting, J. Bao, M. Skyllas-Kazacos, J. Power Sources 203 (2012) 165–176.
[9] A. Tang, J. Bao, M. Skyllas-Kazacos, J. Power Sources 216 (2012) 489–501.
[10] C. Blanc, A. Rufer, 2008 IEEE International Conference on Sustainable Energy Technologies (ICSET), vols. 1 and 2, 2008, pp. 696–701.
[11] N.E. Todreas, M.S. Kazimi, Nuclear Systems, Hemisphere Pub. Corp., New York, 1990.
[12] I.E. Idelchik, E. Fried, Handbook of Hydraulic Resistance, second ed., Hemisphere Pub. Corp., Washington, 1986.
[13] A.A. Shah, M.J. Watt-Smith, F.C. Walsh, Electrochim. Acta 53 (2008) 8087–8100.
[14] C. Blanc, Modeling of a Vanadium Redox Flow Battery Electricity Storage System. PhD thesis (2009).
[15] W.M. Kays, M.E. Crawford, Convective Heat and Mass Transfer, second ed., McGraw-Hill, New York, 1980.
[16] L.F. Moody, Trans. A.S.M.E. (1944) 671–684.
[17] A. Shah, R. Tangirala, R. Singh, R.G.A. Wills, F.C. Walsh, J. Electrochem. Soc. 158 (2011) A671–A677.
[18] X.K. Ma, H.M. Zhang, C.X. Sun, Y. Zou, T. Zhang, J. Power Sources 203 (2012) 153–158.
[19] Y.H. Wen, H.M. Zhang, P. Qian, P. Zhao, H.T. Zhou, B.L. Yi, Acta Phys. Chim. Sin. 22 (2006) 403–408.
[20] N. Kausar, Studies of V(IV) and V(V) Species in Vanadium Cell Electrolyte. PhD thesis, UNSW, 2002.
[21] F. Rahman, M. Skyllas-Kazacos, J. Power Sources 189 (2009) 1212–1219.
[22] P. Zhao, H.M. Zhang, H.T. Zhou, J. Chen, S.J. Gao, B.L. Yi, J. Power Sources 162 (2006) 1416–1420.
[23] B.R. Munson, D.F. Young, T.H. Okiishi, Fundamentals of Fluid Mechanics, third ed., J. Wiley, New York, 1998.
[24] C. Sun, J. Chen, H. Zhang, Y. Zhenkun, Battery Bimonth. 39 (2009) 297–300.
[25] A. Heintz, C. Illenberger, Ber. Bunsen Phys. Chem. 102 (1998) 1401–1409.
[26] M. Skyllas-Kazacos, M. Kazacos, J. Joy, B.G. Madden, Patent Appl. No. PCT/AU89/00252, (June 1989).